Atmospheric Environment 218 (2019) 116982

Contents lists available at ScienceDirect

Atmospheric Environment

journal homepage: www.elsevier.com/locate/atmosenv

Aerosol chemical component: Simulations with WRF-Chem and comparison with observations in Nanjing

Tong Sha[a], Xiaoyan Ma[a,*], Hailing Jia[a], Rong Tian[a], Yunhua Chang[b,c], Fang Cao[b,c], Yanlin Zhang[b,c]

[a] *Collaborative Innovation Center on Forecast and Evaluation of Meteorological Disasters (CIC-FEMD)/Key Laboratory for Aerosol-Cloud-Precipitation of China Meteorological Administration, Nanjing University of Information Science & Technology, Nanjing, 210044, China*

[b] *Yale–NUIST Center on Atmospheric Environment, International Joint Laboratory on Climate and Environment Change (ILCEC), Nanjing University of Information Science & Technology, Nanjing, 210044, China*

[c] *Jiangsu Provincial Key Laboratory of Agricultural Meteorology, College of Applied Meteorology, Nanjing University of Information Science & Technology, Nanjing, 210044, China*

ARTICLE INFO

Keywords:
Inorganic aerosols
$PM_{2.5}$
WRF-Chem
Heterogeneous reactions

ABSTRACT

Secondary inorganic aerosols, including sulfate, nitrate, and ammonium (SNA), are the predominant components of fine particles ($PM_{2.5}$). Reasonable representations of SNA formation in numerical models can largely improve the predictions of $PM_{2.5}$ concentrations and effectively help implement emission control strategies. Despite the Atmospheric Pollution Prevention and Control Action Plan has been implemented since 2013, $PM_{2.5}$ concentration during 2017 in Nanjing, one of the megacities in China, still exceeded the World Health Organization-recommended safe level ($35\,\mu g\,m^{-3}$). In this study, WRF-Chem model was applied to simulate aerosol chemical components in $PM_{2.5}$ during April 2016 and January 2017 in Nanjing, and the simulations are evaluated with in-situ observations. Our results show that the model can reasonably reproduce the temporal variability of $PM_{2.5}$ in two seasons, but significantly underestimate the sulfate concentrations by 71% (84%) in April (January), and overestimate the nitrate concentrations by 67% (45%) in April (January). The simulated ammonium is overall consistent with the observations. Meanwhile, the model tends to overestimate SO_2 concentrations by 20% (74%) in April (January). Several sensitivity studies are conducted to explore the mechanisms for underestimation of sulfate and overestimation of nitrate, and found that the conversion rate of SO_2 to sulfate is significantly underestimated in the model. Tripling the gas-phase oxidation rate of SO_2 by OH only enhances sulfate by 67% (72%) in April (January), indicating gas-phase oxidation is not the main causes for the underestimations in the model. However, inclusion of SO_2 heterogeneous oxidation in aerosol water can largely increase the simulated sulfate by 84% (196%) in April (January), and also better reproduce the diurnal variations of sulfate compared to the reference run. It should be noted that the simulated sulfate is still 47% (53%) lower than the observations in April (January), though inclusion of heterogeneous reaction can substantially improve the simulation performance of SNA.

1. Introduction

In recent years, rapid industrialization and urbanization have caused the frequent occurrence of haze events in East China, such as the North China Plain (NCP) region, the Yangtze River Delta (YRD) region, and the Pearl River Delta (PRD) region. Anthropogenic $PM_{2.5}$ (fine particulate matter with aerodynamic diameters less than 2.5 μm), as the primary pollutant causing haze, is known to play a significant role in atmospheric visibility, human health, and climate (Hyslop, 2009; Yang et al., 2017; Chen et al., 2018a,b,c). Although the $PM_{2.5}$ concentration in YRD has decreased by 34% in the recent 5 years (2013–2017) because of implementation of the Atmospheric Pollution Prevention and Control Action Plan, the annual mean $PM_{2.5}$ over YRD in 2017 still reached $47\,\mu g\,m^{-3}$, which is 1.3 times the World Health Organization-recommended safe level of $35\,\mu g\,m^{-3}$ (https://www.aqistudy.cn/) (Chinese State Council, 2013; Ma and Jia, 2016; Ma et al., 2019). Therefore, understanding the mechanism of haze formation in this region is an urgent task for policymakers.

Secondary inorganic species, including sulfate, nitrate, and ammonium (SNA), are the predominant species in $PM_{2.5}$, and their rapid

---

[*] Corresponding author.
E-mail address: xma@nuist.edu.cn (X. Ma).

https://doi.org/10.1016/j.atmosenv.2019.116982
Received 10 June 2019; Received in revised form 30 August 2019; Accepted 15 September 2019

formation is one of the main causes of haze episodes (Huang et al., 2014; Zheng et al., 2015; Han et al., 2016). Wang et al. (2015) showed that the SNA mass fraction in $PM_{2.5}$ can be up to 50% during severe haze days, which is 1.7 times that during clean days in Nanjing. Many field observations have investigated the rapid formation mechanism of SNA during haze events. Tang et al. (2016) suggested that local chemical transformation associated with high relative humidity (RH) dominates the rapid formation of SNA in Beijing. Yang et al. (2015) argued that local chemical conversion would not be able to explain the observed rapid formation of SNA in a short time. Using a ceilometer and in-situ observation data in Beijing, Zhu et al. (2016) and Ma et al. (2017) further proposed that regional transport was the major cause of the initial haze stage and the local chemical reactions, especially heterogeneous chemistry, dominated the later pollution.

It thus is meaningful to further study the complex formation mechanism of particulate matter. Numerical model is a favorable tool to predict air pollutants and understand physical and chemical processes. However, adequately predicting $PM_{2.5}$ peak concentrations and the proportion of chemical components in $PM_{2.5}$ are still challenging for regional air quality models (Li et al., 2017a,b). Studies show that most models fail to simulate sulfate, nitrate and ammonium concentrations over East Asia, particularly underestimate sulfate and overestimate nitrate (Chen et al., 2016; Cheng et al., 2016; Fu et al., 2016; Gao et al., 2016a; Li et al., 2018). These are mainly caused by the uncertainties in simulated meteorological conditions (Gao et al., 2016b; Sun et al., 2016) and emission inventories (Ma et al., 2018; Sha et al., 2019), as well as unclear and/or inaccurate physical and chemical mechanisms associated with air pollutants in the model (Tuccella et al., 2012; He and Zhang, 2014). Heterogeneous reaction on preexisting aerosols, which is proved to be important for the formation of the winter haze in China (Cheng et al., 2016; Wang et al., 2016a,b), and its impacts on the simulated secondary inorganic aerosols are investigated and found that the discrepancy can be largely reduced by inclusion of heterogeneous chemistry into the model (Zheng et al., 2015; Chen et al., 2016; Li et al., 2017a,b, 2018; Feng et al., 2018). As far as we know, most modeling studies mainly focus on a pollution process during winter or autumn over the North China Plain (NCP) and Guanzhong Basin (GZB), while systematic evaluation of the simulated aerosol chemical components and further exploration of the reasons for discrepancy between simulation and observation in other seasons over YRD are relatively few.

From April 1st to 30th, 2016 and January 16th to 30th, 2017, a field campaign was carried out at Nanjing University of Information Science & Technology (NUIST) in Nanjing, a megacity over YRD, to online measure the gas precursors and aerosol chemical components. In this study, the WRF-Chem model was applied to simulate SO_2, NO_2, NH_3, as well as SNA and $PM_{2.5}$ in the campaign period, and the simulations are compared with the in-situ observations to further investigate the causes of discrepancy during two seasons from the perspective of chemical mechanism. The paper is organized as below. The model configuration and observations used, as well as meteorology evaluation are presented in section 2. The simulation evaluation of chemical fields compared with in-situ observations are presented in section 3. A subsection is dedicated to sensitivity experiments to explore the model bias in the SNA simulation, especially sulfate. Summaries are given in section 4.

2. Model description, data, and model evaluation

2.1. Model description

The Weather Research and Forecasting (WRF) model coupled with online chemistry (WRF-Chem) in version 3.6.1 (Grell et al., 2005) is used in this study. The parameterization schemes for physical processes include Morrison 2-moment (Morrison et al., 2008), Grell 3-D cumulus (Grell and Dezső, 2002), RRTMG (Rapid Radiative Transfer Model for GCMs) short and long wave radiation (Iacono et al., 2008), Noah land surface model, and the Yonsei University planetary boundary layer parameterization (Hong et al., 2006). Gas-phase chemical mechanism CBMZ (Zaveri and Peters, 1999) and 4-bin sectional MOSAIC aerosol model with aqueous chemistry (Zaveri et al., 2008) are chosen. MOSAIC treats all the important aerosol species, including sulfate, nitrate, ammonium, chloride, sodium, BC, primary organic mass, other inorganic mass (OIN), and liquid water. Aerosol water content is calculated using the method by Zdanovskii-Stokes-Robinson (ZSR) (Zdanovskii, 1948; Stokes and Robinson, 1966), and ZSR parameters are derived using the comprehensive Pitzer-Simonson-Clegg model (PSC) (Pitzer and Simonson, 1986; Clegg et al., 1998) at 298.15 K. However, this method is usually found to fail at lower RH values in the atmosphere, especially for the relatively small electrolytes in a given multicomponent solution.

Table 1
The main formation mechanisms of sulfate, nitrate, and ammonium (SNA) in the current model.

	Gas phase	Aqueous phase
Sulfate	$SO_2 + OH \rightarrow H_2SO_4 + HO_2$	$S(IV) + H_2O_2 \rightarrow S(VI)$ $S(IV) + O_3 \rightarrow S(VI)$ $HSO_3^- + 2NO_2 \overset{H_2O}{\rightarrow} SO_4^{2-} + 3H^+ + 2NO_2^-$ $S(IV) + \frac{1}{2}O_2 \overset{Fe^{3+}, Mn^{2+}}{\rightarrow} S(VI)$
Nitrate	$OH + NO_2 \overset{M}{\rightarrow} HNO_3$ $O_3 + NO_2 \rightarrow NO_3 + O_2$ $NO_3 + NO_2 \overset{M}{\rightarrow} N_2O_5$ $N_2O_5 + H_2O \rightarrow 2HNO_3$	$NO_2 + OH \rightarrow H^+ + NO_3^-$ $NO_3 + HO_2 \rightarrow O_2 + NO_3^-$ $NO_3 + O_2^- \rightarrow O_2 + NO_3^-$ $NO_3 + H_2O_2 \rightarrow H^+ + HO_2 + NO_3^-$

In the standard simulation with the CBMZ-MOSAIC mechanism, the sulfate, nitrate, and ammonium aerosols are mainly formed through oxidation and neutralization/condensation of gas precursor. As shown in Table 1, sulfate is produced (SO_2 oxidized to sulfuric acid H_2SO_4) via two pathways, i.e., gas-phase oxidation of SO_2 by OH, and aqueous-phase oxidation of S(IV) ($= SO_2 \cdot H_2O + HSO_3^- + SO_3^{2-}$) by H_2O_2, O_3, NO_2, as well as through O_2 catalyzed by transition metal ions (Fe^{3+}, Mn^{2+}) in cloud droplets. The nitrate formation (NO_x to nitric acid HNO_3 oxidation) also mainly includes two pathways, the NO_2 oxidation by OH during the daytime, and the hydrolysis of dinitrogen pentoxide (N_2O_5) at night (Archer-Nicholls et al., 2014). Note the aqueous-phase oxidation of NO_x in cloud droplets is much less important than the above two pathways (Dentener and Crutzen, 1993; Jacob, 2000). For ammonium, its formation is mainly from the neutralization/condensation of H_2SO_4 and HNO_3 with NH_3 to form ammonium sulfate ($(NH_4)_2SO_4$) or ammonium bisulfate (NH_4HSO_4) and ammonium nitrate (NH_4NO_3), respectively. The extent to which sulfate is neutralized and ammonium nitrate is formed is mainly governed by thermodynamic equilibrium, which is solved by MTEM-MSEA (Multicomponent Taylor Expansion Method and Multicomponent Equilibrium Solver for Aerosols) module used in MOSAIC (Zaveri et al., 2005a;b). The equilibrium is determined by the temperature, relative humidity, and molar concentrations of total sulfate (SO_4^{2-}), total nitrate (HNO_3, NO_3^-), and total ammonia (NH_3, NH_4^+) (Wang et al., 2008a, b). As H_2SO_4 is nonvolatile, sulfate neutralization precedes NH_4NO_3 formation especially under warm conditions, while under cooler temperatures, NH_4NO_3 is formed favorably given sufficient NH_3 although the sulfate is not fully neutralized (Pinder et al., 2008). Since the inorganic aerosol system is essentially an acid-base titration, the amount of NH_3 is a key factor in determining the SNA formation.

The simulation is performed on a domain in 27 km × 27 km horizontal resolution over eastern China and nested to a domain in 9 km × 9 km covering the YRD (Fig. 1), with 30 vertical levels. Initial conditions for meteorological variables are obtained from the National Center for Environmental Prediction's (NCEP) Final Analysis (FNL) dataset (http://rda.ucar.edu/datasets/ds083.2/) with a horizontal resolution of 1° × 1°. The chemical initial and boundary conditions are

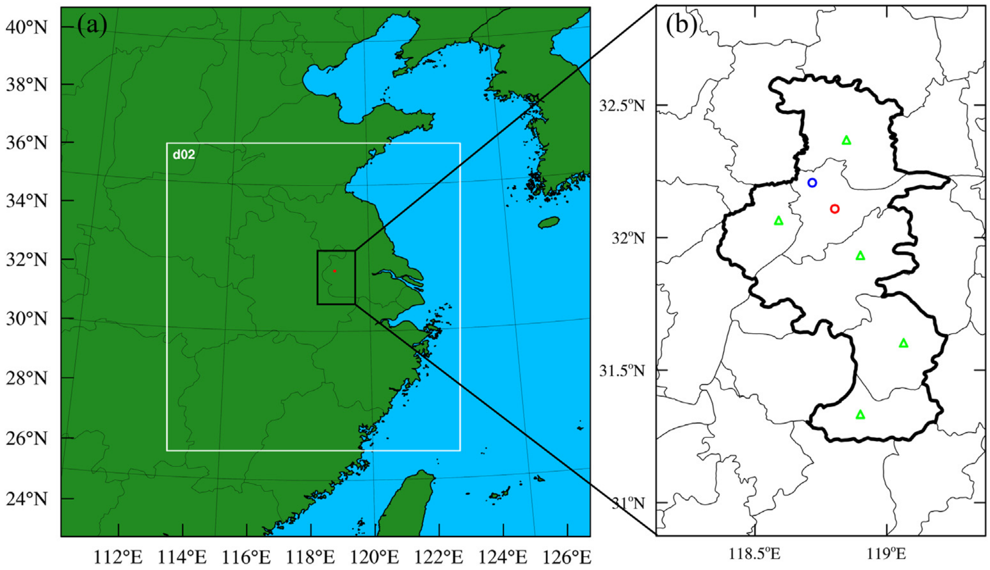

Fig. 1. The model domain (The location of the solid red dot represents Nanjing) (a). The location of sites with in-situ measurements on meteorological variables and air pollutants (Green triangles, red circle, and blue circle denote meteorological stations, Maigaoqiao air quality monitoring site, and Nanjing University of Information Science & Technology (NUIST), respectively) (b). (For interpretation of the references to color in this figure legend, the reader is referred to the Web version of this article).

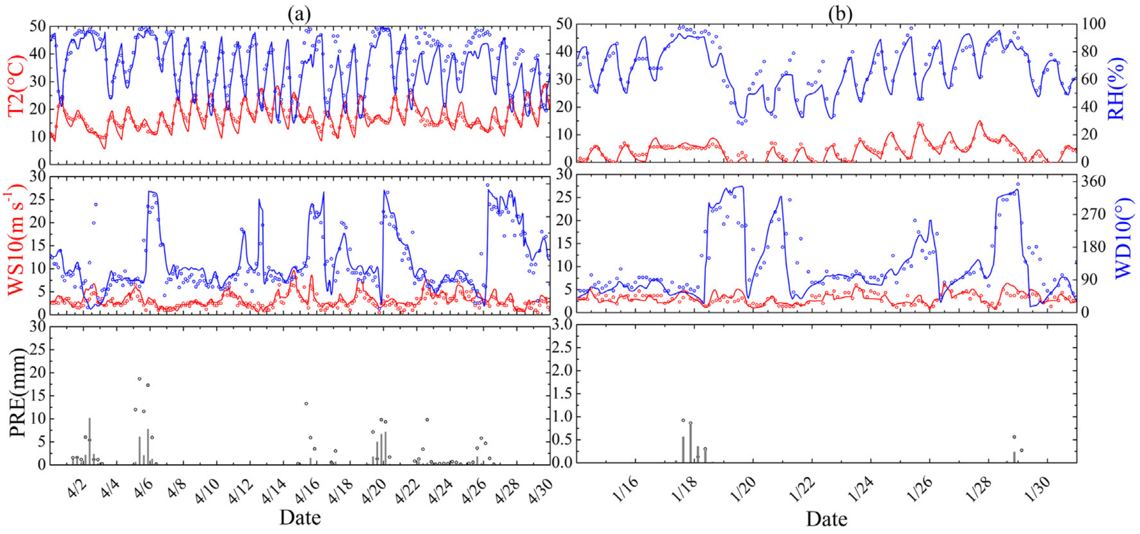

Fig. 2. Time series of the observed and simulated hourly 2 m temperature (T2), 2 m relative humidity (RH), 10 m wind speed (WS10), 10 m wind direction (WD10), and 6 h accumulation precipitation (PRE) during April 2016 (a) and January 2017(b) in Nanjing. (Scatters and solid lines (or columns) represent observations and simulations, respectively).

provided by the Model for Ozone and Related chemical Tracers, version 4 (MOZART-4) (Emmons et al., 2010). The anthropogenic emissions are taken from Multi-resolution Emission Inventory for China (MEIC: http://www.meicmodel.org/) for the year 2016, which is a bottom-up inventory framework developed by Tsinghua University (Li et al., 2017a,b). The simulations started on March 30th, 2016 and December 30th, 2016, and ended up on April 30th, 2016 and January 31st, 2017, the first 2 days are treated as a spin-up period and not used in our analyses.

2.2. Observational data

The meteorological data in 5 meteorological sites in Nanjing were taken from the Meteorological Information Comprehensive Analysis and Process System (MICAPS), shown as green triangles in Fig. 1(b). The following variables are evaluated, including temperature and relative humidity at 2 m (T2 and RH), wind speed and direction at 10 m (WS10 and WD10) and 6 h accumulated precipitation (PRE). The sample frequency is 3 h except for precipitation. The observed surface air pollutants are from two data sets: (1) the hourly mass concentrations of SO_2, NH_3 and inorganic chemical components in $PM_{2.5}$ (including sulfate, nitrate, and ammonium) measured by the Monitor for AeRosols and GAses in ambient air (MARGA, Metrohm Applikon B.V., the Netherlands) (Brink et al., 2007) at Nanjing University of Information Science & Technology (NUIST), shown as the blue circle in Fig. 1(b); (2) the hourly mass concentrations of NO_2 and $PM_{2.5}$ at Maigaoqiao monitoring site in Nanjing from the China National Environmental Monitoring Center (CNEMC), shown as the red circle in Fig. 1(b) (because the NUIST site did not simultaneously observe NO_2 and $PM_{2.5}$, the observation data of Maigaoqiao site nearest to the NUIST were selected). The observations values from monitoring station are compared with the mean results of the nearest model grids.

2.3. Model evaluation

The meteorological condition is critical to influence the simulated air pollutants and their temporal and spatial distribution. It thus is essential to evaluate the modeled meteorological variables with respect to the observations during the same period. The statistical metrics calculated include the mean value, standard deviation (σ), temporal

Table 2
Statistics of meteorological simulations during April 2016 and January 2017 in Nanjing. (T2: temperature at 2 m (°C), RH: relative humidity at 2 m (%), WS10: wind speed at 10 m (m s^{-1}), WD10: wind direction at 10 m (°)).

Date	April 2016					January 2017				
Var	Obs (σ)	Mod (σ)	R	MB	RMSE	Obs (σ)	Mod (σ)	R	MB	RMSE
T2	17.41 (4.0)	17.38 (4.7)	0.93	−0.03	1.8	4.04 (3.3)	4.01 (3.4)	0.91	−0.03	1.2
RH	75.9 (17.7)	69.9 (18.1)	0.90	−6.0	10.2	69.0 (16.9)	68.0 (16.7)	0.88	−1.0	7.7
WS10	2.8 (1.4)	3.3 (1.6)	0.79	0.5	1.1	3.0 (1.1)	3.1 (1.2)	0.65	0.1	0.9
WD10	140.9 (74.6)	148.9 (79.8)	0.83	8.0	46.2	138.1 (78.6)	124.6 (91.7)	0.84	−13.5	55.0

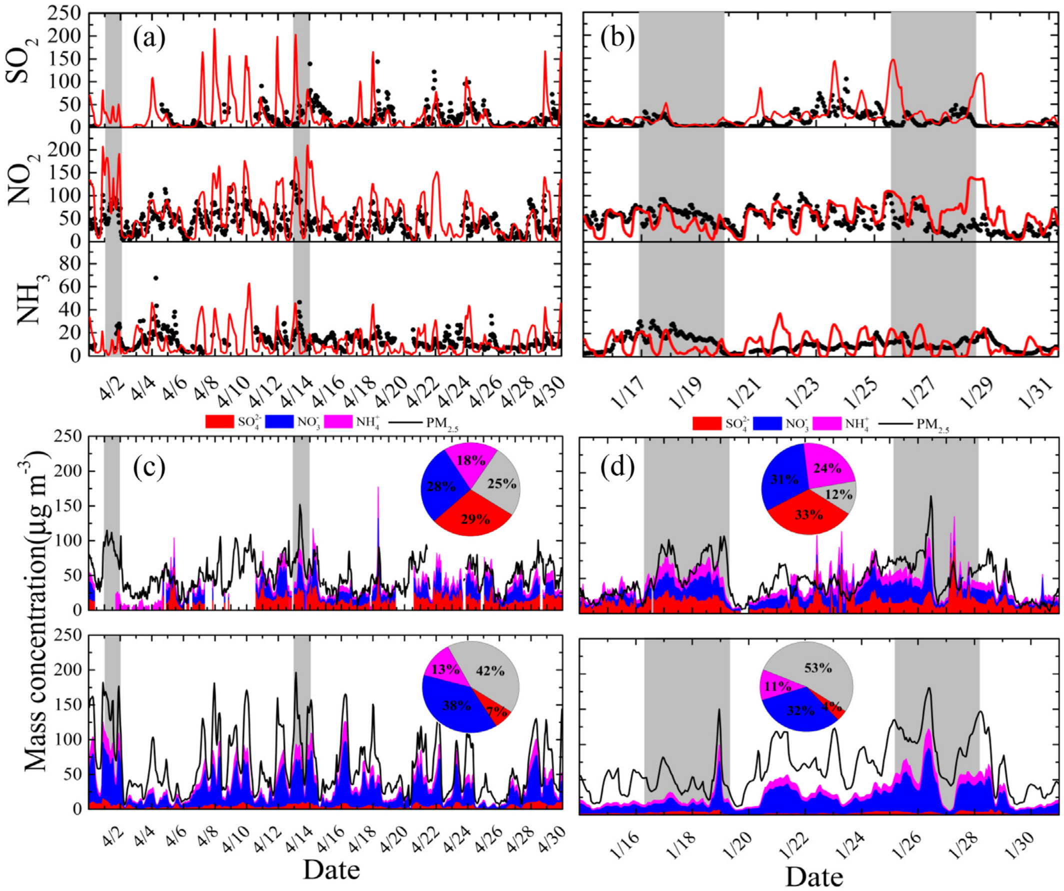

Fig. 3. Time series of the observed and simulated hourly gas precursor (SO_2, NO_2, NH_3) concentrations during April 2016 (a) and January 2017 (b) in Nanjing. (The black dots and solid red lines correspond to the observations and simulations, respectively.) Time series of the observed and simulated sulfate, nitrate and ammonium (SNA) and $PM_{2.5}$ during April 2016 (c) and January 2017 (d) in Nanjing. (The subgraphs above and below represent the observed and simulated results, respectively. Pie charts show the proportion of SNA in $PM_{2.5}$, and the gray part represents the other components in $PM_{2.5}$.). (For interpretation of the references to color in this figure legend, the reader is referred to the Web version of this article).

Table 3
The mean concentrations (μg m^{-3}) and standard deviations (σ, μg m^{-3}) (in brackets) of pollutants from observations and simulations during April 2016 and January 2017 in Nanjing. Correlation coefficients (R) and normalized mean bias (NMB, %) between observations and simulations are also shown in the table.

	April				January			
	Obs	Mod	R	NMB	Obs	Mod	R	NMB
SO_2	20.2(21.4)	24.3(34.1)	0.12	20.3	14.1(15.7)	24.5(28.7)	0.13	73.8
NO_2	41.9(25.7)	60.4(46.8)	0.53	64.4	47.3(22.4)	55.1(30.1)	0.34	16.5
NH_3	12.4(6.9)	11.6(10.4)	0.11	−6.5	10.6(6.0)	10.0(8.3)	0.10	−5.7
Sulfate	14.9(7.8)	4.3(2.9)	0.26	−71.4	15.9(10.5)	2.5(1.6)	0.31	−84.3
Nitrate	14.7(9.2)	24.5(19.7)	0.32	66.7	14.8(9.3)	21.4(15.6)	0.51	44.6
Ammonium	9.5(5.0)	8.3(6.5)	0.31	−12.6	11.2(7.1)	7.4(4.8)	0.27	−33.9
$PM_{2.5}$	51.1(23.4)	64.7(44.1)	0.55	26.6	47.4(27.0)	66.0(35.8)	0.58	39.2

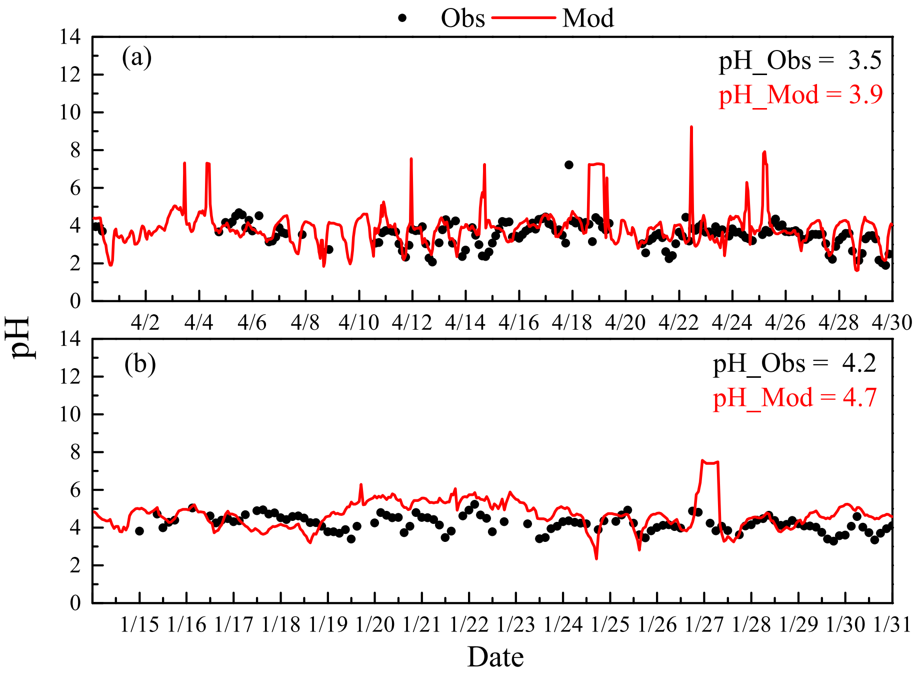

Fig. 4. Time series of the observed and simulated $PM_{2.5}$ pH during April 2016 (a) and January 2017 (b) in Nanjing, calculated using ISORROPIA II and the hourly chemical concentrations of observations (the black dots) and simulations (the solid red lines). (For interpretation of the references to color in this figure legend, the reader is referred to the Web version of this article).

Table 4
Mean values of the simulated and observed meteorological fields, hourly air pollutant concentrations during EP3 and EP4 in Nanjing.

		EP3		EP4	
		Obs	Mod	Obs	Mod
Mete	T2	5.7	5.8	6.8	6.4
	RH2	81.8	82.0	73.5	72.5
	WS10	2.8	2.7	2.5	2.8
	WD10	75.6	64.7	154.6	157.7
Chem	SO_2	12.7	18.5	10.8	46.3
	NO_2	71.9	53.9	52.6	78.5
	NH_3	20.9	10.1	11.3	13.3
	Sulfate	22.7	3.7	17.0	3.5
	Nitrate	23.3	14.7	28.6	50.5
	Ammonium	17.1	6.1	16.2	14.9
	OIN	–	16.2	–	30.0
	$PM_{2.5}$	77.8	57.1	83.6	126.6

correlation coefficient (R), mean bias (MB), normalized mean bias (NMB) and the root mean square error (RMSE). The definitions of these metrics can be found in Lu et al. (1997) and Boylan and Russell (2006).

Fig. 2 compares the temporal variations of simulated and observed meteorological variables. It is seen that the temporal variation of meteorological variables are captured quite well by the model, with the correlations during two seasons ranging 0.91–0.93, 0.88–0.90, 0.65–0.79, and 0.83–0.84 for the 2 m temperature (T2), 2 m relative humidity (RH), 10 m wind speed (WS10) and direction (WD10), respectively. As shown in Table 2, T2 and RH are slightly lower than observations, with the biases less than 0.03 °C and 6% in two seasons, respectively, while WS10 is overestimated by 0.5 $m\,s^{-1}$ in April and 0.1 $m\,s^{-1}$ in January. Seven precipitation processes were found during April, although the model could capture the starting and ending time, but underestimates the precipitation by 2.6 mm. The precipitation during January was quite limited, and weak precipitation occurred only on January 18th to 19th and 29th, which the model could also reproduce well. Overall, the statistics suggest that the simulated meteorological is overall reasonable in Nanjing. The overestimated wind speed may lead to some biases of the air pollutant concentrations, and the underestimated T2 and RH may also cause negative biases of temperature-dependent and/or RH-dependent reaction coefficients in the simulations.

3. Results and discussions

3.1. Chemical simulations

Fig. 3 shows the time series of observed and simulated SO_2, NO_2, NH_3, as well as SNA and $PM_{2.5}$. The magnitudes and trends over time of the simulated air pollutants are generally consistent with observations. Four regional haze episodes, i.e., daily $PM_{2.5}$ concentration reached 75 $\mu g\,m^{-3}$, are identified on April 2nd (EP1), 14th (EP2) and January 17th-18th (EP3), 26th-27th (EP4) in Nanjing. The model can generally capture the four haze episodes, but significantly underestimates sulfate concentrations by over 70% in both seasons, especially in winter, with the NMB of −84%. In the meantime, the simulated SO_2 concentrations are 20% (74%) higher than the observations during April (January) (see Table 3). A few possibilities might contribute to the discrepancies. First, there exist some uncertainties in emission inventory, though the baseline year of inventory is consistent with the year of simulation. The bottom-up approach analyzes and integrates SO_2-related activity rates (of coal power plants, industry, and residential combustion) with SO_2 emission factors from various agencies and sources, and it thus has limitations in that it usually has a temporal lag and can quickly become outdated, especially in developing countries (Wang et al., 2016a,b), which result in high SO_2 emissions in inventory. Second, the low conversion rate of SO_2 to sulfate in the current model version can result in the discrepancies of both SO_2 and sulfate. Third, typical measurement systems for ambient aerosols easily misinterpret organosulfur (mainly in the presence of hydroxy-methane sulfonate (HMS)) as inorganic sulfate, thus leading to a positive observational bias, e.g., mean bias during winter haze in Beijing is 20% (Moch et al., 2018; Song et al., 2019).

Compared to SO_2 and sulfate, the model overestimates NO_2 and nitrate concentrations by 17%–64% and 45%–67%, respectively, 'during two seasons (see Table 3). The underestimation of sulfate and overestimation of nitrate, i.e., nitrate substitution paradox, may arise from a positive bias in aerosol pH in model simulations, due to that aerosol acidity can drive the semi-volatile partitioning of key aerosol species (Guo et al., 2015; Weber et al., 2016). Vasilakos et al. (2018)

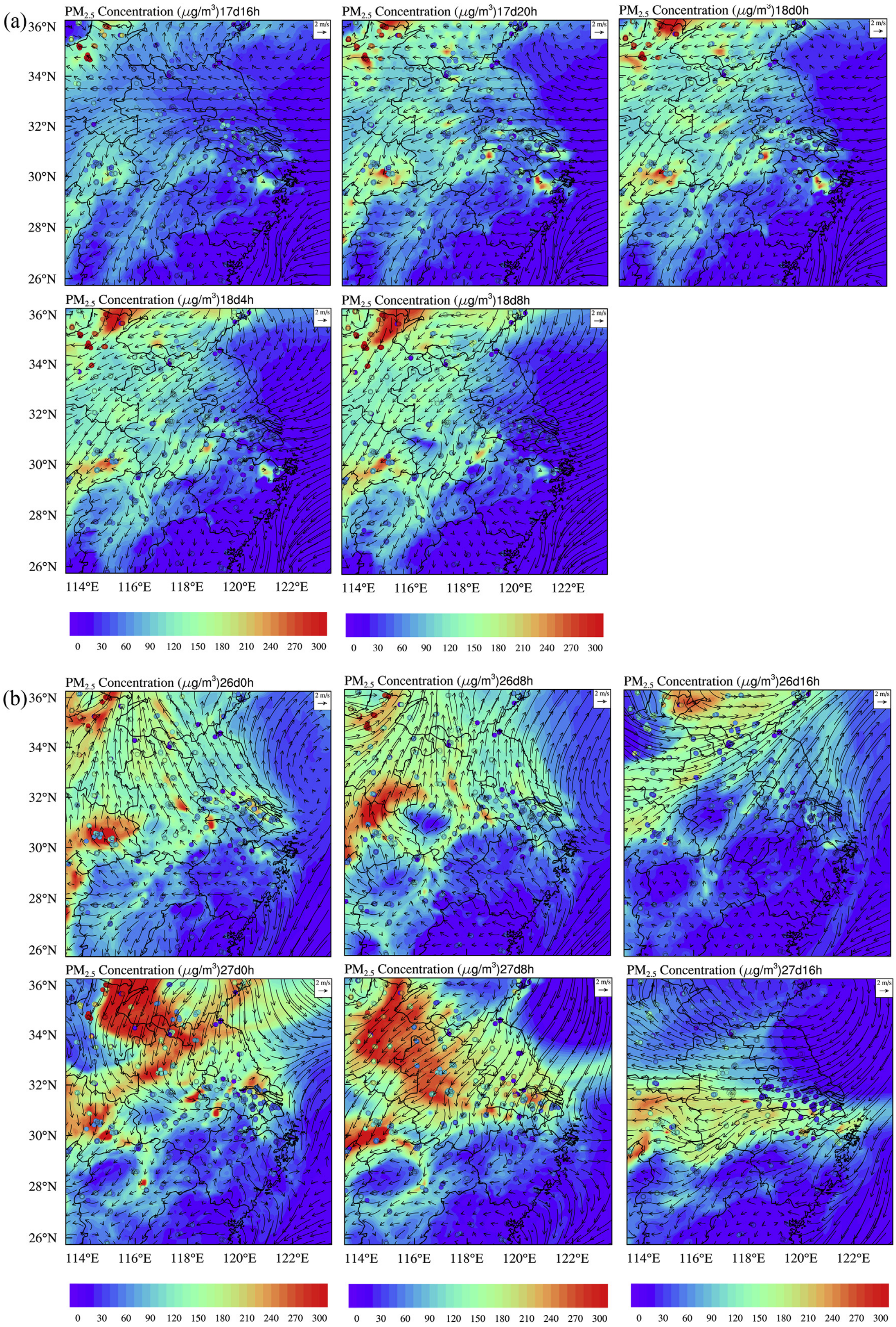

Fig. 5. Time series of spatial distribution for the simulated and observed surface $PM_{2.5}$ concentration (μg m^{-3}) and wind field (m s^{-1}) during 5 selected times in EP3 (January 17th to18th) (a) and 6 selected times in EP4 (January 26th to 27th) (b) over YRD. (The circles represent the observed surface $PM_{2.5}$ concentrations, and the black arrows indicate the simulated surface wind fields).

Table 5
Description of the model simulations.

Experiment	Description
Reference	Reference run.
Gas3	SO_2 gas-phase oxidation rate was tripled from the reference run.
Het	Heterogeneous sulfate formation is added into WRF-Chem, and the reaction is as follow: $SO_2(gas) + aerosol \rightarrow SO_4^{2-}$

found that nonvolatile cations (NVCs: K^+, Na^+, Ca^{2+}, and Mg^{2+}) in the fine mode are responsible for the erroneous predicted increase in aerosol pH of about 1 unit on average over America, and such an increase can induce a nitrate bias of 1–2 μg m^{-3}. The comparisons of the simulated and observed $PM_{2.5}$ pH calculated using ISORROPIA II (Fountoukis and Nenes, 2007) are shown in Fig. 4. As the CBMZ-MOSAIC version used is not capable of simulating NVCs, the effects of NVCs on pH are eliminated by assuming that the simulated NVCs concentrations are consistent with the observations. However, the simulated $PM_{2.5}$ pH is still higher than the observations in both seasons, with the biases of 0.4 in April and 0.5 in January. Therefore, the positive biases of $PM_{2.5}$ pH can explain the overestimation of nitrate to some extent, but not enough to explain such a large bias (10 μg m^{-3} in April and 7 μg m^{-3} in January). In addition, overestimating the NO_x emissions in MEIC inventory and underestimating the dry/wet deposition of total nitric acid (HNO_3 and nitrate) in the model may partly lead to these positive discrepancies.

The model can overall predict the NH_3 concentration (the NMB less than 7%), but is unable to capture its variability. This is due to lacking accurate and latest coefficients of diurnal variation of NH_3 emissions, and the setting of coefficients in the model are obtained from the investigation results (the baseline year is 2008) of Zhai et al. (2012), which may deviate from the current situation. Compared to sulfate and nitrate, the simulated ammonium is relatively reasonable in both seasons, with the biases lower than 34% (see Table 3).

The simulated $PM_{2.5}$ is quite consistent with observations in two seasons, with the temporal correlation coefficients (R) ranging from 0.55 to 0.58 and the NMB ranging from 27% to 39% (see Table 3). Considering that the model underestimates the proportion of SNA mass concentrations in $PM_{2.5}$ by 17% (41%) in April (January), and also underestimates organic mass concentrations due to that CBMZ-MOSAIC only treats primary organic species but not predicts secondary organic aerosols formation (Gao et al., 2016b). Therefore, the overestimation of $PM_{2.5}$ is mainly due to the overestimation of OIN. Noted that the model significantly underestimates the sulfate proportion, it thus is important to understand the key mechanism of sulfate formation, and more detailed analysis will be shown in section 3.2.

The two haze episodes occurred on January 17th −18th (EP3, mean $PM_{2.5}$ of 78 μg m^{-3}) and 26th - 27th (EP4, mean $PM_{2.5}$ of 84 μg m^{-3}) were selected to further explore the reasons for the discrepancy between simulation and observation (Fig. 3(d)). The model can reasonably capture the timing of pollution buildups during EP3, but underestimates $PM_{2.5}$ concentrations by 27%, which is mainly caused by much lower simulated SNA (the NMB of −84%, −37%, and −64% for sulfate, nitrate, and ammonium, respectively) (see Table 4). In addition, the humid eastern wind from sea prevailed during this period in Nanjing (Fig. 5(a)), and the relative humidity and surface temperature had no obvious diurnal variation, so this episode was mainly caused by local pollution. Compared to EP3, the simulated $PM_{2.5}$ in EP4 is 51% higher than the observations. Because the SNA mass concentrations from simulated (69 μg m^{-3}) and observed (62 μg m^{-3}) are quite close, the overestimation of $PM_{2.5}$ is possibly due to the overestimation of primary $PM_{2.5}$. According to Fig. 5(b), the southerly wind prevailed at 00:00 on the 26th and clean airflow in the upstream area dispersed the pollution previously generated in Nanjing. Starting from 00:00 on the 27th, the wind direction turned to the north, the strong and cold northwesterly airflow brought air pollutants from the highly polluted NCP, thereby leading to this haze event over YRD .

3.2. *Sensitivity experiments*

As stated above, the discrepancies of SO_2 and sulfate are probably due to high SO_2 emissions in the inventories and low conversion rate of SO_2 to sulfate in the model. Some possibilities might contribute to the low conversion rate. First, the reaction rate of SO_2 gas-phase oxidation might be slow due to the uncertainties of the simulated OH concentrations (Lu et al., 2013; Tan et al., 2017) and oxidation rate constant (Tuccella et al., 2012). The recommended value of rate constant is 1.3×10^{-12} cm^{-3} molecule^{-1} s^{-1} in the most recent comprehensive evaluation for atmospheric chemistry (Atkinson et al., 2004; Long et al., 2017), which is slightly higher than the simulated rate constant (the mean value of 0.9×10^{-12} cm^{-3} molecule^{-1} s^{-1}) in this study. Second, SO_2 heterogeneous reactions in aerosol water are not included in the current model (Zheng et al., 2015; Chen et al., 2016). Several heterogeneous reaction pathways have been proposed, including the oxidation of SO_2 by NO_2 (Gao et al., 2016a; Cheng et al., 2016; Wang et al., 2016a,b, 2018; Li et al., 2018), O_2 catalyzed by transition metal ions (TMIs) (Li et al., 2011, 2017a,b; Shao et al., 2019), and via a free radical chain mechanism (Huie and Neta, 1984; Hung and Hoffmann, 2015). However, the heterogeneous mechanism is still poorly characterized and the relative importance of these multiple pathways still remains highly uncertain, partly due to uncertainties in the aerosol water content, pH, and ionic strength (Herrmann et al., 2015; Cheng et al., 2016). Latest studies show that heterogeneous sulfate formation is dominated by TMIs-catalyzed oxidation of SO_2, based on the fact that aerosol pH is always acidic (pH of 4–5) in China regardless of ammonia levels (Guo et al., 2017; Song et al., 2018; Shao et al., 2019). Third, in-cloud sulfate production might be underestimated due to the uncertainties of the simulated cloud properties and the solubility for gas traces (e.g., SO_2, H_2O_2, and O_3). Therefore, two sensitivity experiments are conducted, as listed in Table 5. The reference run is the simulation discussed in section 3.1.

In the experiment Gas3, the gas-phase oxidation rate of SO_2 by OH was tripled to evaluate the impact of this process on sulfate production. In the experiment Het, a relatively simple SO_2 heterogeneous reaction in aerosol water was added into the CBMZ-MOSAIC chemical mechanism due to the limitations in the current understanding of the heterogeneous mechanism. This reaction is parameterized using the pseudo-first-order rate constant and assumed to be irreversible (Zhang and Carmichael, 1999). The rate constant k (s^{-1}) for the loss of gaseous pollutants is calculated using probability formulation in Jacob (2000) and Wang et al. (2012) (Eq. (1)).

$$k = \left(\frac{d_p}{2D} + \frac{4}{\nu\gamma}\right)^{-1} S_p \tag{1}$$

where d_p is the effective diameter of the particles (m). D, ν and γ are the gas-phase molecular diffusion coefficient (m^2 s^{-1}), mean molecular speed in the gas phase (m s^{-1}) and uptake coefficient (dimensionless) for SO_2, respectively. S_p is the aerosol surface area per unit volume of air (m^{-2} m^{-3}). The parameter γ is obtained using a similar method as Zheng et al. (2015) and Chen et al. (2016). The lower and upper limits of γ are used to present a range in the laboratory measurements which are applied when RH is lower than 50% and higher than 90%, respectively. The values in the 50–90% RH range are linearly interpolated based on the two limits. The lower and upper limits are 2.0×10^{-5} and 5.0×10^{-5}, respectively, which are based on Chen et al. (2016).

3.2.1. *Gas-phase chemistry*

Fig. 6 shows the simulated SNA and $PM_{2.5}$ concentrations in Gas3 and reference run, and comparisons with observations. As shown in

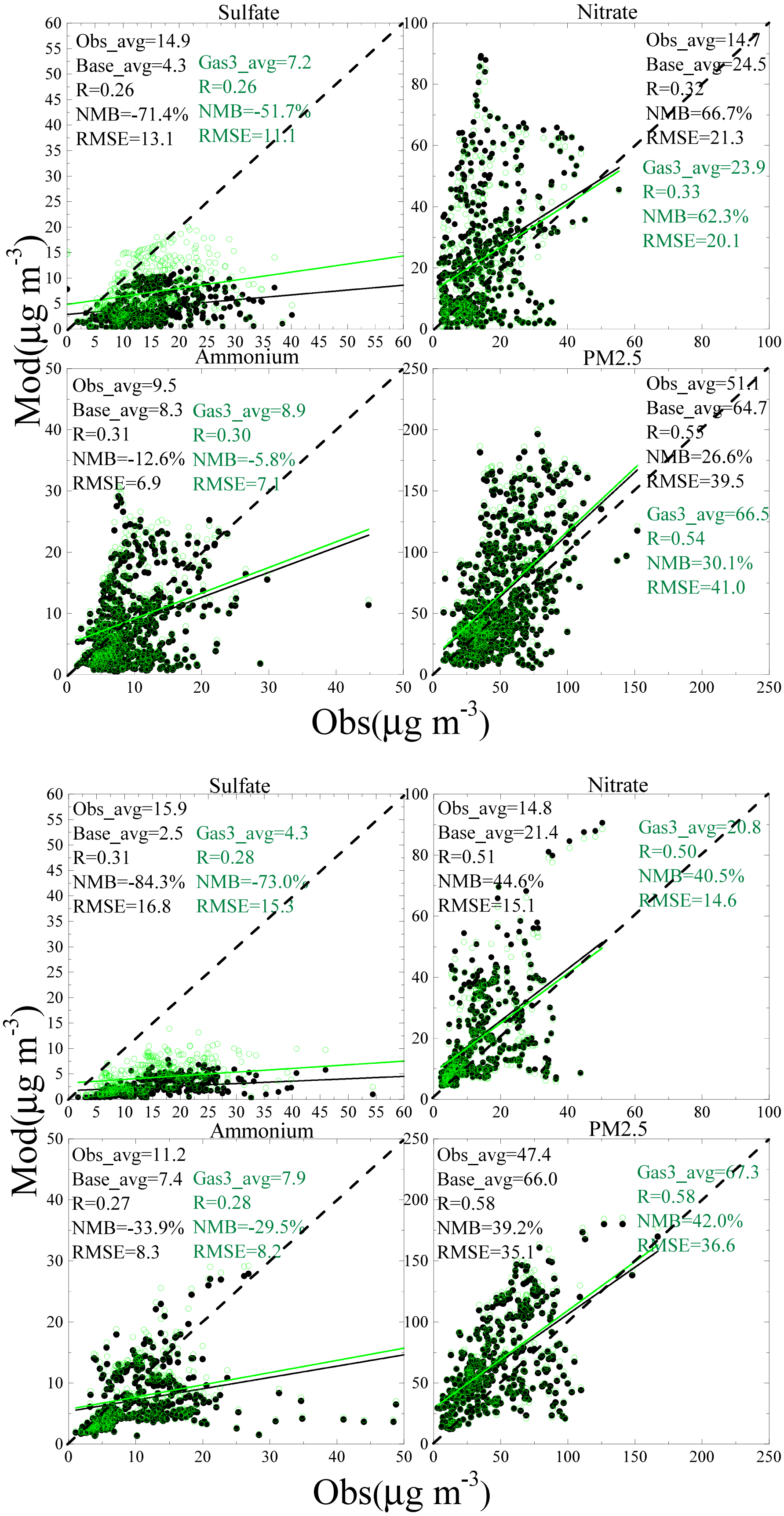

Fig. 6. Scatter plots of the simulated hourly sulfate, nitrate, ammonium (SNA) and $PM_{2.5}$ concentrations with the observed values during April 2016 (a) and January 2017(b) in Nanjing. The black and green dots represent the results of simulations in Reference and Gas3 versus observations, respectively. (For interpretation of the references to color in this figure legend, the reader is referred to the Web version of this article).

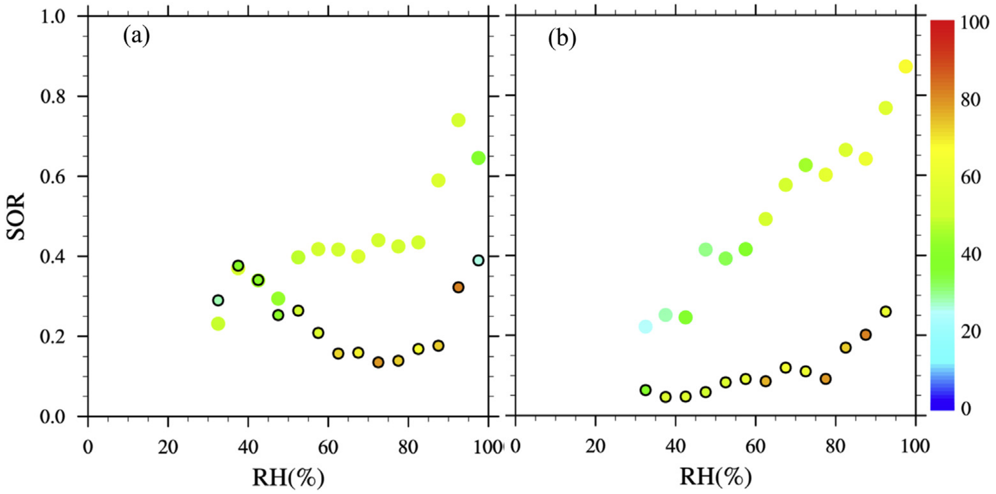

Fig. 7. The relationship between SOR and RH during April 2016 (a) and January 2017 (b) in Nanjing. The circles without and with black border indicate the observations and simulations (in the reference run), respectively, and are colored according to the $PM_{2.5}$ concentrations.

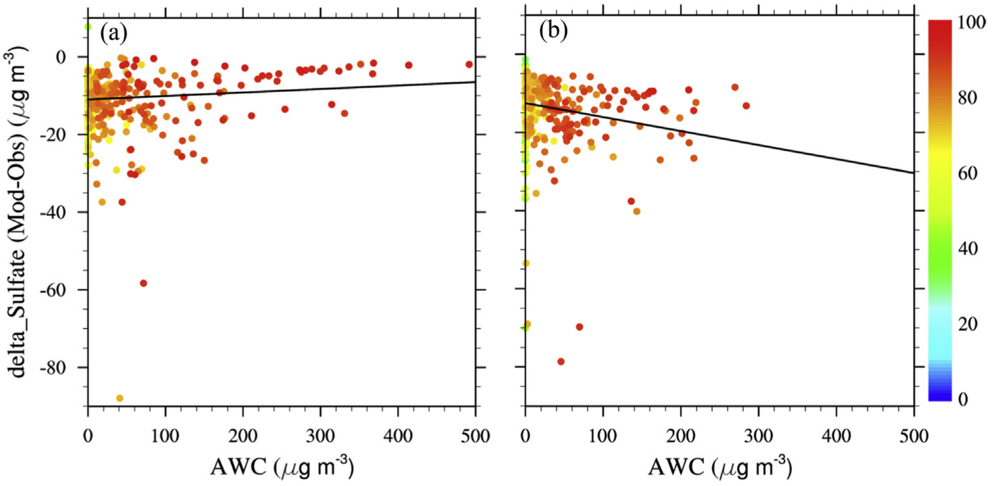

Fig. 8. The relationship between the biases of sulfate (the simulated values minus the observed values) and the simulated aerosol water content (AWC) during April 2016 (a) and January 2017 (b) in Nanjing. The simulations are in the reference run. The circles are colored according to relative humidity, and black lines represent the line fit.

Fig. 6, sulfate concentrations increased 3 μg m^{-3} (67%) in April and 2 μg m^{-3} (72%) in January compared to the reference run, with the NMB reducing by 20% in April and 11% in January, respectively. However, the simulated sulfate is still over 50% lower than the observations, especially in winter (the NMB of −73%), indicating gas-phase oxidation is not the main causes for the sulfate underestimations in the model. In addition, the simulated nitrate only decreases by 0.6 μg m^{-3} (4%) in both seasons with respect to the reference run. Since the simulated $PM_{2.5}$ pH changes slightly in Gas3 compared to the reference run, and is higher than the observations in two seasons (Fig. A1), the positive bias in aerosol pH in model simulations may lead to the nitrate substitution paradox. The modest increment of sulfate production in Gas3 is not surprising, because the lifetime of SO_2 against the oxidation by OH is 7–14 days, and SO_2 oxidation mainly occurs in the aqueous phase (Jacob, 1999; Harris et al., 2013).

3.2.2. SO_2 heterogeneous reaction

The sulfur oxidation ratio () (n refers to the molar concentration) is used to indicate the gaseous species oxidation rate and the secondary transformation (Sun et al., 2006, 2013). The observed high sulfate concentrations during polluted episodes are often related to the high SOR. Fig. 7 shows the observed and simulated SOR (in the reference run). In April, the observations show that SOR overall increases with RH, while the simulated SOR is much lower than the observations when RH is higher than 50%. In January, the observed SOR drastically increases and is strongly correlated with high $PM_{2.5}$ concentrations, but the simulated SOR increases slowly and thus the discrepancy between the observed and simulated become larger with the increase of RH. These findings suggest that the underestimation of sulfate is possibly due to missing the related SO_2 oxidation reaction in aqueous-phase, especially in high environmental humidity. From the relationship between the biases of sulfate and the simulated aerosol water content (AWC) (Fig. 8), we can see that the relationship in April is quite weak, but the biases increase with AWC in January. These could explain why the negative bias of sulfate in January is larger than in April, possibly due to missing SO_2 heterogeneous reaction in aerosol water in the current model, which is considered to be one of the important mechanisms for the winter haze formation (Chen et al., 2016, 2018a,b,c; Gao et al., 2016a).

The simulated results in Het shown in Fig. 9, indicates that the inclusion of SO_2 heterogeneous reaction increases the simulated sulfate by 4 μg m^{-3} (84%) in April and 5 μg m^{-3} (196%) in January, with the NMB reducing by 24% in April and 31% in January, respectively. Due to the sulfate production from heterogeneous chemistry strongly affected by SO_2 concentrations and relative humidity (because the uptake coefficient γ is RH-dependent), the sulfate is overestimated when SO_2 peak concentrations are abnormally high, such as on April 8th, 9th and January 29th. While the simulated sulfate does not enhance too much when the RH is underestimated (e.g., January 17th −19th, 22nd −25th and April 23rd-26th, and the NMBs of RH are −6%, −7% and

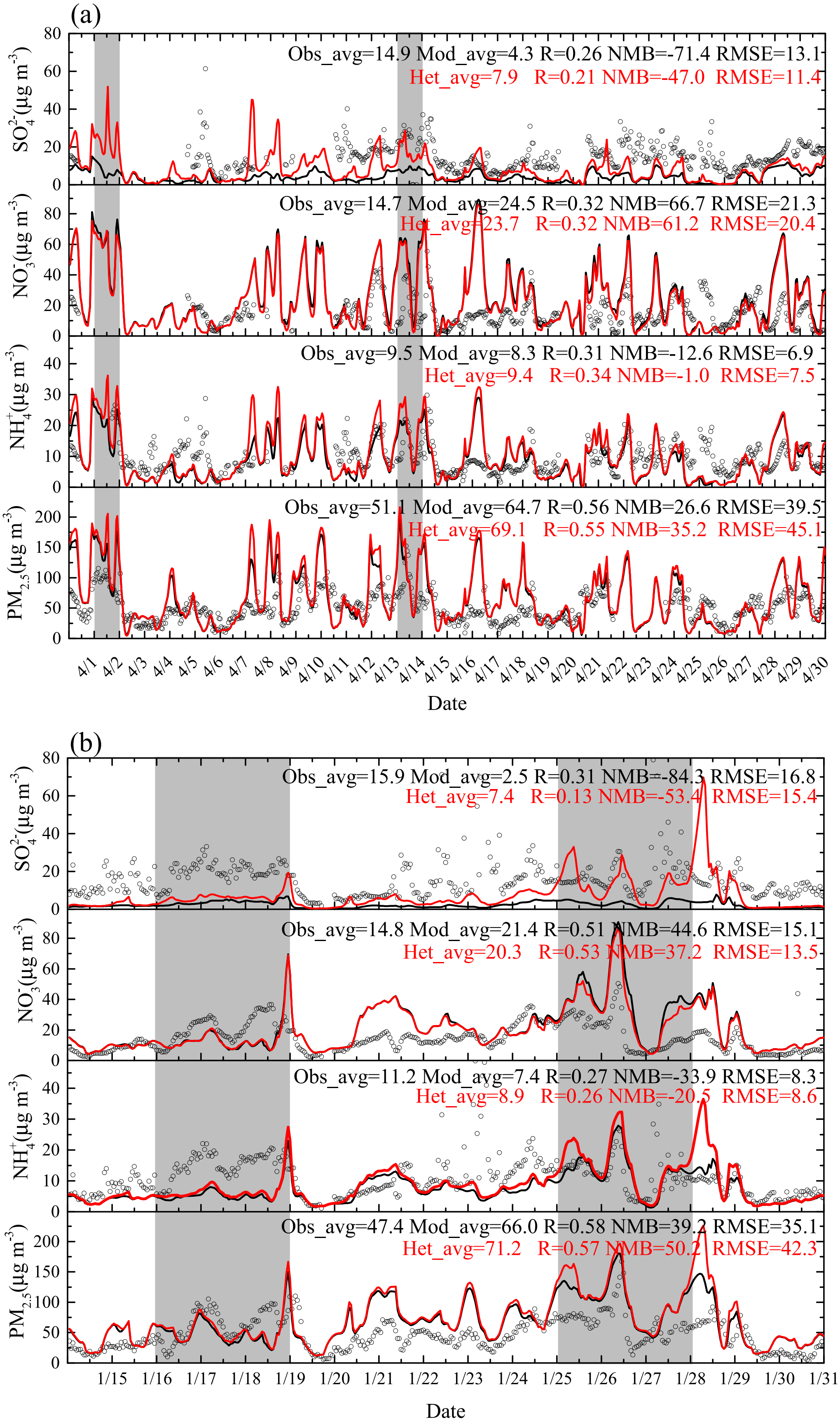

Fig. 9. Comparison of the observed and simulated hourly sulfate, nitrate, ammonium (SNA) and $PM_{2.5}$ concentration during April 2016 (a) and January 2017 (b) in Nanjing. The black hollow circles correspond to the observations, and the solid black and red lines are the simulations in Reference and Het, respectively. (For interpretation of the references to color in this figure legend, the reader is referred to the Web version of this article).

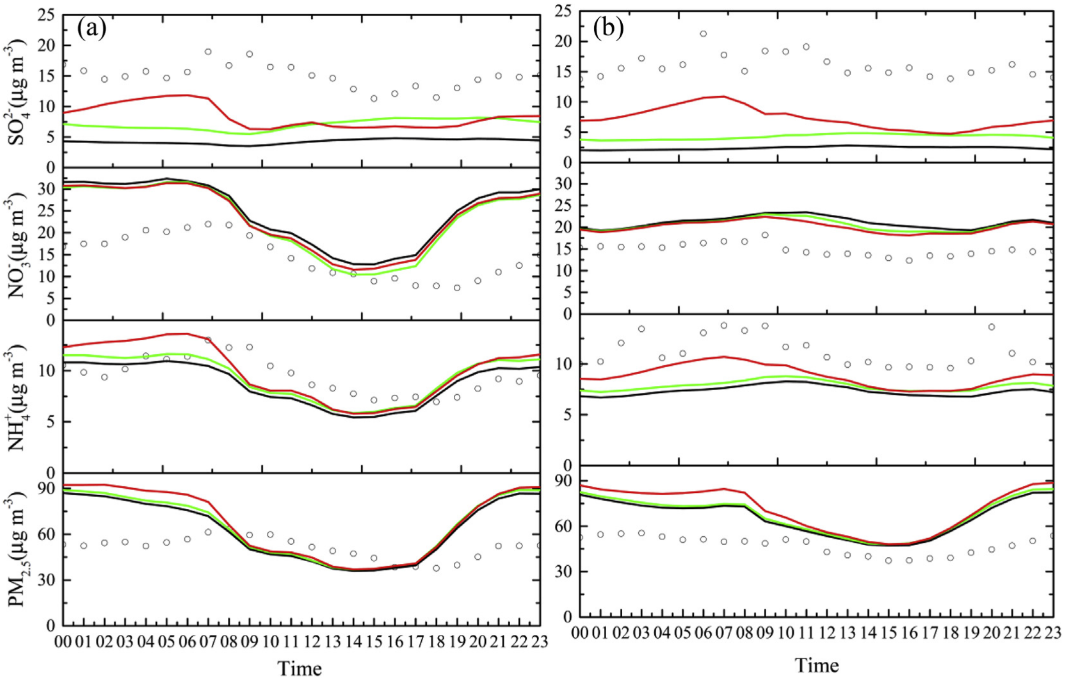

Fig. 10. The observed and simulated diurnal cycles of mass concentrations of sulfate, nitrate, ammonium (SNA) and $PM_{2.5}$ averaged during April 2016 (a) and January 2017 (b) in Nanjing. The black hollow circles correspond to the observations, the solid black, green and red lines are the simulations in Reference, Gas3, and Het, respectively. (For interpretation of the references to color in this figure legend, the reader is referred to the Web version of this article).

−17%, respectively). It is noted that the correlation coefficients between the simulated and observed sulfate in Het decrease from 0.26 to 0.21 in April and 0.31 to 0.13 in January compared with the reference run, most likely due to several abnormal values of the simulated sulfate in two seasons. In addition, the simulated nitrate concentrations reduce slightly by 0.8 μg m^{-3} (3%) in April and 1.1 μg m^{-3} (5%) in January, respectively, against with the reference run. These could be explained by that the simulated $PM_{2.5}$ pH in Het is still higher than the observations and the nitrate substitution paradox still exists. The simulation performance of ammonium is also improved, with the NMB reducing by 12% (13%) in April (January), indicating that sulfate aerosols play an important role in ammonium formation. However, inclusion of SO_2 heterogeneous reaction enlarges the discrepancy between simulation and observation in $PM_{2.5}$, mainly because the increase of simulated sulfate cannot effectively decrease the nitrate concentrations in NH_3-rich conditions, such as Nanjing. Furthermore, the coefficients of nitrate, ammonium and $PM_{2.5}$ simulated by Het are not much different from the reference run.

Diurnal variations of particles concentrations in Fig. 10 show that the simulated SNA and $PM_{2.5}$ in Het can reasonably reproduce the diurnal variations of both SNA and $PM_{2.5}$, particularly for sulfate, which is not seen in the reference run and Gas3 experiments. These results indicate that the chemical mechanism in the current model version cannot account for the daytime and nighttime formation of sulfate in Nanjing, while the inclusion of heterogeneous reaction dissolved SO_2 in aerosol water can reproduce a better diurnal variation.

As discussed earlier, inclusion of SO_2 heterogeneous can obviously improve the sulfate simulation, i.e., largely reduce the biases between the simulations and observations, and better reproduce the diurnal variations, especially in January. But it should be noted that the simulated sulfate is still lower than the observations (the NMB of −47% and −53% in April and January, respectively).

We acknowledge that heterogeneous reactions included in the model are quite simple. For instance, the upper limit for SO_2 uptake coefficient might be too low, and the parameters, such as aerosol liquid water content, pH, and ionic strength, which certainly impact on heterogeneous reaction rates (Herrmann et al., 2015; Cheng et al., 2016; Shao et al., 2019), are not considered in the parameterization scheme. Furthermore, in-cloud aqueous-phase chemical production, an important source of sulfate aerosol (Barth et al., 2000; Alexander et al., 2012; Chen et al., 2018a,b,c), is possibly underestimated to some extent in the model. Previous studies showed that in-cloud oxidation of SO_2 in the global stratiform cloud can contribute 61% of the total sulfate production (Ma and Salzen, 2006). Aan de Brugh et al., 2011 estimated that 45% of SO_2 aqueous oxidation to sulfate over Europe happens within the boundary layer, which may certainly have an important impact on surface concentrations. In CBMZ-MOSAIC mechanism, in-cloud sulfate production depends on the availability of SO_2, H_2O_2, O_3, and NO_2 for the oxidation rate formulations (given in Table 1), as well as the ambient temperature, pH of the cloud water, cloud droplet size, liquid water path (LWP) and cloud fractions (CFs). The uncertainties of these factors can significantly influence the in-cloud production of sulfate. Cloud droplet is an important medium for aqueous-phase reactions, so the accurate simulation of LWP and CFs is very crucial (Wang et al., 2013). Comparisons of the simulated LWP and CFs with satellite observations from the AMSR-E (the Advanced Microwave Scanning Radiometer - EOS) shown in Fig. 11 indicate that the trend of simulated LWP is consistent with the observations, but the model generally underestimates LWP and CFs in both seasons. For example, the satellite observations are cloudy on April 4th, 10th, 21st, 25th, 27th, 28th, and 29th and January 15th, 20th, 23rd, 25th, 27th, 28th, 30th, and 31st, while the model results are clear on the same days. Therefore, the underestimated LWP and CFs can also lead to underestimating the in-cloud sulfate formation, resulting in the simulated sulfate much lower than the observations.

4. Summary

Accurately predicting the concentration and composition of particulate matter is still very challenging in climate and air quality models. In this study, the WRF-Chem model was used to simulate aerosol chemical components in $PM_{2.5}$ during April 2016 and January 2017 in Nanjing. Our objective is to better understand the physical and chemical processes impacting aerosol compositions and concentrations by

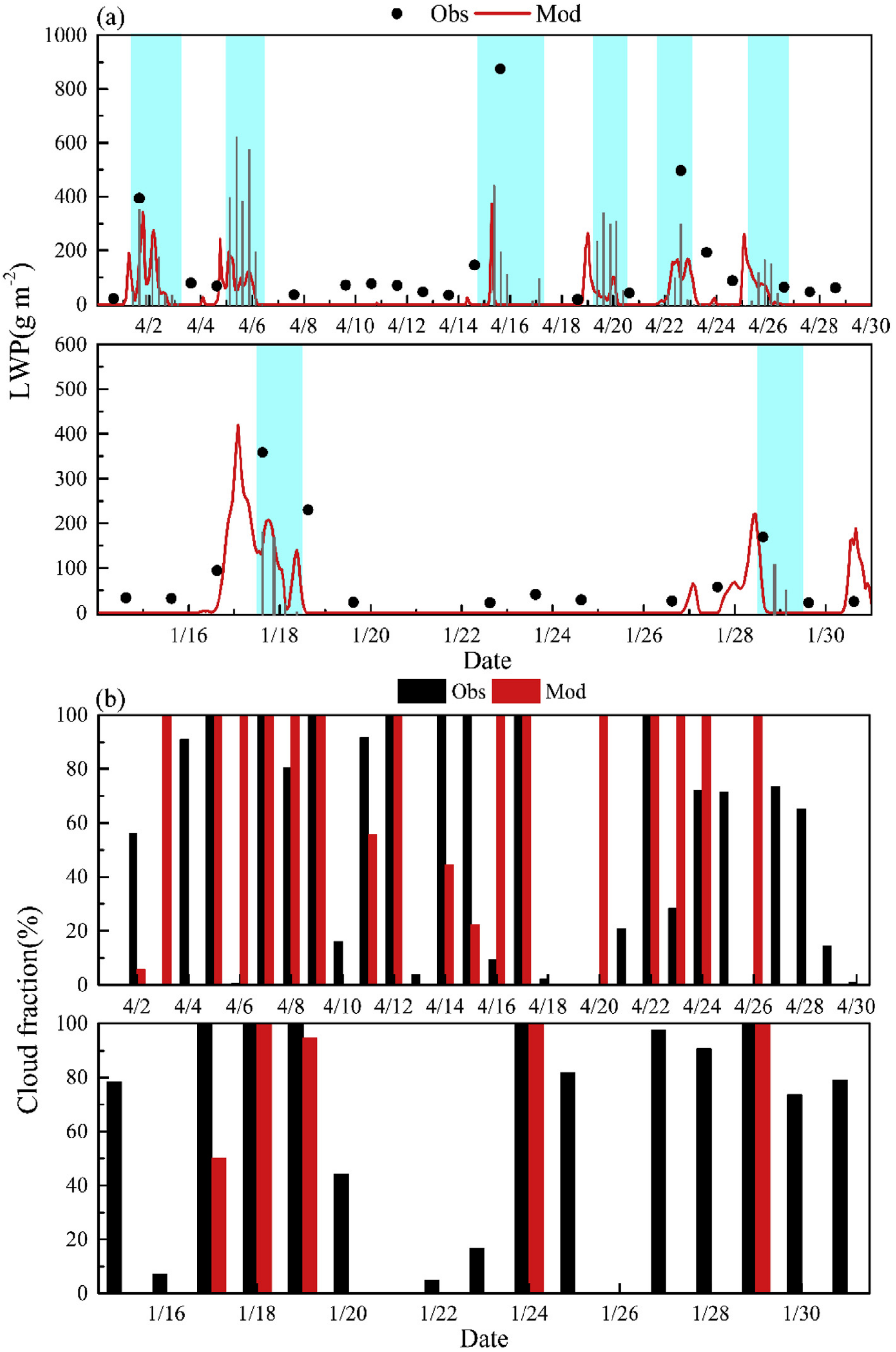

Fig. 11. Temporal variations of the observed and simulated liquid water path (LWP) (a) and cloud fractions (CFs) (b) during April 2016 and January 2017 in Nanjing. The black columns (solid dots) and red columns (solid lines) correspond to the observations and simulations (in the reference run), respectively. The blue shadow and gray columns in Fig. (a) represent the time period of precipitation. (For interpretation of the references to color in this figure legend, the reader is referred to the Web version of this article).

looking into the discrepancies between the simulations and observations.

Compared with the in-situ observations, the CBMZ-MOSAIC mechanism in WRF-Chem can reasonably simulate temporal variations of SO_2, NO_2, NH_3, and $PM_{2.5}$ and reproduce four haze episodes in two seasons. However, the model significantly underestimates sulfate concentrations over 70%, especially in January (the negative bias of 84%), and overestimates 45–67% nitrate. The model can reasonably predict ammonium concentrations in both seasons, with the biases lower than 34%. Meanwhile, the simulated SO_2 concentrations are 27% (74%) higher than the observations in April (January), suggesting that SO_2 emissions are possibly high in the emission inventories and the conversion rate of SO_2 to sulfate is too slow in the model.

We conducted two sensitivity experiments to explore the large discrepancies of sulfate mentioned above, i.e., tripling gas-phase oxidation rate of SO_2 by OH (Gas3), and incorporating SO_2 heterogeneous reaction (Het). The results suggest that tripling SO_2 gas-phase oxidation rate does not significantly enhance sulfate concentrations. Compared with the reference run, the Gas3 only increase sulfate by 67% in April and 72% in January, while the Het can obviously increase sulfate by 84% in April and 196% in January, and also better reproduce the observed diurnal variations of sulfate.

However, the simulated sulfate in Het is still 47% in April and 53% in January lower than the observations. These suggest that physical and chemical mechanisms in the current model version need further improved for better agreement with the observations. For example, the upper limit for SO_2 uptake coefficient might be low. The impact of parameters (e.g., aerosol liquid water content, pH, and ionic strength) on heterogeneous reaction rates are not considered in the parameterization. In addition, the lower liquid water path and cloud fractions in the model could lead to relatively weak in-cloud sulfate production, and thus lower sulfate mass. More studies are necessary to further improve the simulations of aerosol chemical composition in the future.

Declaration of competing interest

The authors declare that they have no known competing financial interests or personal relationships that could have appeared to influence the work reported in this paper.

Acknowledgments

This study is supported by the National Natural Science Foundation of China grants (41675004), the National Key R&D Program of China grants (2016YFA0600404), and the funding of Jiangsu Innovation & Entrepreneurship Team.

Appendix A. Supplementary data

Supplementary data to this article can be found online at https://doi.org/10.1016/j.atmosenv.2019.116982.

References

Aan de Brugh, J.M.J., Schaap, M., Vignati, E., Dentener, F., Kahnert, M., Soviev, M., Huijnen, V., Krol, M.C., 2011. The European aerosol budget in 2006. Atmos. Chem. Phys. 11, 1117–1139.

Alexander, B., Allman, D.J., Amos, H.M., Fairlie, T.D., Dachs, J., Hegg, D.A., Sletten, R.S., 2012. Isotopic constraints on the formation pathways of sulfate aerosol in the marine boundary layer of the subtropical northeast Atlantic Ocean. J. Geophys. Res. Atmos. 117, D06304.

Archer-Nicholls, S., Lowe, D., Utembe, S., Allan, J., Zaveri, R.A., Fast, J.D., Hodnebrog, Ø., Denier van der Gon, H., McFiggans, G., 2014. Gaseous chemistry and aerosol mechanism developments for version 3.5.1 of the online regional model. WRF Chem. Geosci. Model Dev. 7, 2557–2579.

Atkinson, R., Baulch, D.L., Cox, R.A., Crowley, J.N., Hampson, R.F., Hynes, R.G., Jenkin, M.E., Rossi, M.J., Troe, J., 2004. Evaluated kinetic and photochemical data for atmospheric chemistry: volume I – gas phase reactions of Ox, HOx, NOx and SOx species Atmos. Chem. Phys. 2004 (4), 1461–1738 (Experimental data are summarized on page 1637).

Barth, M.C., Rasch, P.J., Kiehl, J.T., Benkovitz, C.M., Schwartz, S.E., 2000. Sulfur chemistry in the national center for atmospheric Research community climate model: description, evaluation, features and sensitivity to aqueous chemistry. J. Geophys. Res. Atmos. 105, 1387–1415.

Boylan, J.W., Russell, A.G., 2006. PM and light extinction model performance metrics, goals, and criteria for three-dimensional air quality models. Atmos. Environ. 40 (26), 4946–4959.

Brink, H.T., Otjes, R., Jongejan, P., Slanina, S., 2007. An instrument for semi-continuous monitoring of the size-distribution of nitrate, ammonium, sulphate and chloride in aerosol. Atmos. Environ. 41 (13), 2768–2779.

Chen, D., Liu, Z., Fast, J., Ban, J.M., 2016. Simulations of sulfate–nitrate–ammonium (SNA) aerosols during the extreme haze events over northern China in October 2014. Atmos. Chem. Phys. 16 (16), 10707–10724.

Chen, Q., Sherwen, T., Evans, M., Alexander, B., 2018a. DMS oxidation and sulfur aerosol formation in the marine troposphere: a focus on reactive halogen and multiphase chemistry. Atmos. Chem. Phys. 18, 13617–13637.

Chen, X.W., Li, X.D., Yuan, X.Z., Zeng, G.M., Liang, J., Li, X., Luo, Y., Chen, G.J., 2018b. Effects of human activities and climate change on the reduction of visibility in Beijing over the past 36 years? Environ. Int. 116, 92–100.

Chen, Y., Wolke, R., Ran, L., Birmili, W., Spindler, G., Schröder, W., Su, H., Cheng, Y.F., Tegen, I., Wiedensohler, A., 2018c. A parameterization of the heterogeneous hydrolysis of N2O5 for mass-based aerosol models: improvement of particulate nitrate prediction. Atmos. Chem. Phys. 18, 673–689.

Cheng, Y.F., Zheng, G.J., Wei, C., Mu, Q., Zheng, B., Wang, Z.B., Gao, M., Zhang, Q., He, K.B., Gregory, R.C., Ulrich, P., Su, H., 2016. Reactive nitrogen chemistry in aerosol water as a source of sulfate during haze events in China. Sci. Adv. 2 (12) 1601530-1601530.

Chinese State Council Atmospheric pollution prevention and control action plan (in Chinese)), last access on 05/27/2019). http://www.gov.cn/zwgk/2013-09/12/content_2486773.htm.

Clegg, S.L., Brimblecombe, P., Wexler, A.S., 1998. Thermodynamic model of the system $H^{+}–NH4^{+}–Na^{+}–SO4^{2-}–NO^{3—}Cl^{-}–H_2O$ at 298.15 K. J. Phys. Chem. B 102, 2155–2171.

Dentener, F.J., Crutzen, P.J., 1993. Reaction of N2O5 on tropospheric aerosols: impact on the global distributions of NOx, O3, and OH. J. Geophys. Res. Atmos. 98 (D4), 7149–7163.

Emmons, L.K., Walters, S., Hess, P.G., Lamarque, J.F., Pfister, G.G., Fillmore, D., Granier, C., Guenther, A., Kinnison, D., Laepple, T., Orlando, J., Tie, X., Tyndall, G., Wiedinmyer, C., Baughcum, S.L., Kloster, S., 2010. Description and evaluation of the model for ozone and related chemical Tracers, version 4 (MOZART-4). Geosci. Model Dev. 3, 43–67.

Feng, T., Bei, N.F., Zhao, S.Y., Wu, J.R., Li, X., Zhang, T., Cao, J.J., Zhou, W.J., Li, G.H., 2018. Wintertime nitrate formation during haze days in the Guanzhong basin, China: a case study. Environ. Pollut. 243, 1057–1067.

Fountoukis, C., Nenes, A., 2007. ISORROPIA II: a computationally efficient thermodynamic equilibrium model for $K^{+}– Ca^{2+}–Mg^{2+}–NH^{4+} –Na^{+}–SO4^{2-} –NO3^{-} –Cl^{-} –H_2O$ aerosols. Atmos. Chem. Phys. 7, 4639–4659.

Fu, X., Wang, S.X., Chang, X., Cai, S.Y., Xing, J., Hao, J.J., 2016. Modeling analysis of secondary inorganic aerosols over China: pollution characteristics, and meteorological and dust impacts. Sci. Rep-UK. 6 (1), 35992.

Gao, M., Carmichael, G.R., Wang, Y.S., Ji, D.S., Liu, Z.R., Wang, Z.F., 2016a. Improving simulations of sulfate aerosols during winter haze over northern China: the impacts of heterogeneous oxidation by NO2. Front. Environ. Sci. Eng. 10 (5).

Gao, M., Carmichael, G.R., Wang, Y.S., Saide, P.E., Yu, M., Liu, Z.R., Wang, Z.F., 2016b. Modeling study of the 2010 regional haze event in the North China Plain. Atmos. Chem. Phys. 15 (16).

Grell, G.A., Dezső, D., 2002. A generalized approach to parameterizing convection combining ensemble and data assimilation techniques. Geophys. Res. Lett. 29, 1693.

Grell, G.A., Peckham, S.E., Schmitz, R., Mckeen, S.A., Frost, G., Skamarock, W.C., Eder, B., 2005. Fully coupled "online" chemistry within the WRF model. Atmos. Environ. 39 (37), 6957–6975.

Guo, H.Y., Weber, R.J., Nenes, A., 2017. High levels of ammonia do not raise fine particle pH sufficiently to yield nitrogen oxide-dominated sulfate production. Sci. Rep-UK 7 (1), 12109.

Guo, H.Y., Xu, L., Bougiatioti, A., Cerully, K.M., Capps, S.L., Hite Jr., J.R., Carlton, A.G., Lee, S.H., Bergin, M.H., Ng, N.L., Nenes, A., Weber, R.J., 2015. Fine-particle water and pH in the southeastern United States. Atmos. Chem. Phys. 15, 5211–5228.

Han, B., Zhang, R., Yang, W., Bai, Z.P., Ma, Z.Q., Zhang, W.J., 2016. Heavy haze episodes in Beijing during January 2013: inorganic ion chemistry and source analysis using highly time-resolved measurements from an urban site. Sci. Total Environ. 544, 319–329.

Harris, E., Sinha, B., van Pinxteren, D., Tilgner, A., Fomba, K.W., Schneider, J., Roth, A., Gnauk, T., Fahlbusch, B., Mertes, S., Lee, T., Collett, J., Foley, S., Borrmann, S., Hoppe, P., Herrmann, H., 2013. Enhanced role of transition metal ion catalysis during in-cloud oxidation of SO2. Science 340, 727–730.

He, J., Zhang, Y., 2014. Improvement and further development in CESM/CAM5: gas-phase chemistry and inorganic aerosol treatments. Atmos. Chem. Phys. 14 (17), 9171–9200.

Herrmann, H., Schaefer, T., Tilgner, A., Styler, S.A., Weller, C., Teich, M., Otto, T., 2015. Tropospheric aqueous-phase chemistry: kinetics, mechanisms, and its coupling to a changing gas phase. Chem. Rev. 115, 4259–4334.

Hong, S.Y., Noh, Y., Dudhia, J., 2006. A new vertical diffusion package with an explicit treatment of entrainment processes. Mon. Weather Rev. 134 (9), 2318.

Huang, R.J., Zhang, Y., Bozzetti, C., Ho, K.F., Cao, J.J., Han, Y.M., Daellenbach, K.R., Slowik, J.G., Platt, S.M., Canonaco, F., Zotter, P., Wolf, R., Pieber, S.M., Bruns, E.A., Crippa, M., Ciarelli, G., Piazzalunga, A., Schwikowski, G., Abbaszade, M., Schnelle-Kreis, J., Zimmermann, R., An, Z.S., Szidat, S., Baltensperger, U., Haddad, I.E., Prévôt, A.S.H., 2014. High secondary aerosol contribution to particulate pollution during haze events in China. Nature 514 (7521), 218–222.

Huie, R.E., Neta, P., 1984. Chemical behavior of $SO3^{-}$ and $SO5^{-}$ radicals in aqueous solutions. J. Phys. Chem. 88, 5665–5669.

Hung, H.M., Hoffmann, M.R., 2015. Oxidation of gas-phase SO2 on the surfaces of acidic microdroplets: implications for sulfate and sulfate radical anion formation in the atmospheric liquid phase. Environ. Sci. Technol. 49, 13768–13776.

Hyslop, N.P., 2009. Impaired visibility: the air pollution people see. Atmos. Environ. 43 (1), 182–195.

Iacono, M.J., Delamere, J.S., Mlawer, E.J., Shephard, M.W., Clough, S.A., Collins, W.D., 2008. Radiative forcing by long-lived greenhouse gases: calculations with the AER radiative transfer models. J. Geophys. Res. Atmos. 113 (D13).

Jacob, D.J., 1999. Introduction to Atmospheric Chemistry. Princeton Univ. Press, Princeton, N. J, pp. 266.

Jacob, D.J., 2000. Heterogeneous chemistry and tropospheric ozone. Atmos. Environ. 34, 2131–2159.

Li, J., Chen, X.S., Wang, Z.F., Du, H.Y., Yang, W.Y., Sun, Y.L., Hu, B., Li, J.J., Wang, W., Wang, T., Fu, P.Q., Huang, H.L., 2018. Radiative and heterogeneous chemical effects of aerosols on ozone and inorganic aerosols over East Asia. Sci. Total Environ. 622–623, 1327–1342.

Li, M., Zhang, Q., Kurokawa, J.-i., Woo, J.-H., He, K.B., Lu, Z.F., Ohara, T., Song, Y., Streets, D.G., Carmichael, G.R., Cheng, Y.F., Hong, C.P., Huo, H., Jiang, X.J., Kang, S., Liu, F., Su, H., Zheng, B., 2017a. MIX: a mosaic Asian anthropogenic emission inventory under the international collaboration framework of the MICS-Asia and HTAP. Atmos. Chem. Phys. 17, 935–963.

Li, W.J., Zhou, S.Z., Wang, X.F., Xu, Z., Yuan, C., Yu, Y.C., Zhang, Q.Z., Wang, W.X., 2011. Integrated evaluation of aerosols from regional brown hazes over northern China in winter: concentrations, sources, transformation, and mixing states. J. Geophys. Res. 116, D09301.

Li, G.H., Bei, N.F., Cao, J.J., Hu, R.J., Wang, J.R., Feng, T., Wang, Y.C., Liu, S.X., Zhang, Q., Tie, X.X., Molina, L.T., 2017b. A possible pathway for rapid growth of sulfate during haze days in China. Atmos. Chem. Phys. 17, 3301–3316.

Long, B., Bao, J.L., Truhlar, D.G., 2017. Reaction of SO2 with OH in the atmosphere. Phys. Chem. Chem. Phys. 19.

Lu, K.D., Hofzumahaus, A., Holland, F., 2013. Missing OH source in a suburban environment near Beijing: observed and modelled OH and HO2 concentrations in summer 2006. Atmos. Chem. Phys. 13, 1057–1080 2013.

Lu, R., Turco, R.P., Jacobson, M.Z., 1997. An integrated air pollution modeling system for urban and regional scales: 2. simulations for SCAQS 1987. J. Geophys. Res. Atmos. 102.

Ma, Q.X., Wu, Y.F., Zhang, D.Z., Wang, X.J., Xia, Y.J., Liu, X.Y., Tian, P., Han, Z.W., Xia, X.G., Wang, Y., Zhang, R.J., 2017. Roles of regional transport and heterogeneous reactions in the PM2.5 increase during winter haze episodes in Beijing. Sci. Total Environ. 599–600, 246–253.

Ma, X., Jia, H.L., 2016. Particulate matter and gaseous pollutions in three megacities over China: situation and implication. Atmos. Environ. 140, 476–494.

Ma, X., Jia, H.L., Sha, T., An, J.L., Tian, R., 2019. Spatial and seasonal characteristics of particulate matter and gaseous pollution in China: implications for control policy. Environ. Pollut. 248, 421–428.

Ma, X., Salzen, K.V., 2006. Dynamics of the sulphate aerosol size distribution on a global scale. J. Geophys. Res. Atmos. 111 (D8).

Ma, X., Sha, T., Wang, J., Jia, H.L., Tian, R., 2018. Investigating impact of emission inventories on PM2.5 simulations over North China Plain by WRF-Chem. Atmos. Environ. 195, 125–140.

Moch, J.M., Dovrou, E., Mickley, L.J., Keutsch, F.N., Cheng, Y., Jacob, D.J., Jiang, J.K., Li, M., Munger, J.W., Qiao, X.H., Zhang, Q., 2018. Contribution of hydroxymethane sulfonate to ambient particulate matter: a potential explanation for high particulate sulfur during severe winter haze in Beijing. Geophys. Res. Lett. 45 (11), 979 969–11.

Morrison, H., Pinto, J.O., Curry, J.A., McFarquhar, G.M., 2008. Sensitivity of modeled arctic mixed-phase stratocumulus to cloud condensation and ice nuclei over regionally varying surface conditions. J. Geophys. Res. Atmos. 113 (D5).

Pinder, R.W., Dennis, R.L., Bhave, P.V., 2008. Observable indicators of the sensitivity of PM2.5 nitrate to emission reductions-Part I: derivation of the adjusted gas ratio and applicability at regulatory-relevant time scales. Atmos. Environ. 42 (6), 1275–1286.

Pitzer, K.S., Simonson, J.M., 1986. Thermodynamics of multicomponent, miscible, and ionic systems: theory and equations. J. Phys. Chem. 90, 3005–3009.

Sha, T., Ma, X.Y., Jia, H.L., van der A, R.J., Ding, J.Y., Zhang, Y.L., Chang, Y.H., 2019. Exploring the influence of two inventories on simulated air pollutants during winter over the Yangtze River Delta. Atmos. Environ. 206, 170–182.

Shao, J.Y., Chen, Q.J., Wang, Y.X., Lu, X., He, P.Z., Sun, Y.L., Shah, V., Martin, R.V., Philip, S., Song, S.J., Zhao, Y., Xie, Z.Q., Zhang, L., Alexander, B., 2019. Heterogeneous sulfate aerosol formation mechanisms during wintertime Chinese haze events: air quality model assessment using observations of sulfate oxygen isotopes in Beijing. Atmos. Chem. Phys. 19, 6107–6123.

Song, S.J., Gao, M., Xu, W.Q., Shao, J.Y., Shi, G.L., Wang, S.X., Wang, Y.X., Sun, Y.L., McElroy, M.B., 2018. Fine-particle pH for Beijing winter haze as inferred from different thermodynamic equilibrium models. Atmos. Chem. Phys. 18, 7423–7438.

Song, S.J., Gao, M., Xu, W.Q., Sun, Y.L., Worsnop, D.R., Jayne, J.T., Zhang, Y.Z., Zhu, L., Li, M., Zhou, Z., Cheng, C.L., Lv, Y.B., Wang, Y., Peng, W., Xu, X.B., Lin, N., Wang, Y.X., Wang, S.X., Munger, J.W., Jacob, D.J., McElroy1, M.B., 2019. Possible heterogeneous chemistry of hydroxymethanesulfonate (HMS) in northern China winter haze. Atmos. Chem. Phys. 19, 1357–1371.

Stokes, R.H., Robinson, R.A., 1966. Interaction in aqueous nonelectrolyte solution. Part I: solute-solvent equilibria. J. Phys. Chem. 70, 2126–2130.

Sun, K., Liu, H.N., Ding, A.J., Wang, Y.X., 2016. WRF-chem simulation of a severe haze episode in the Yangtze River Delta, China. Aerosol air. Qual. Res. 16, 1268–1283.

Sun, Y.L., Wang, Z.F., Fu, P.Q., Yang, T., Jiang, Q., Dong, H.B., Li, J., Jia, J.J., 2013. Aerosol composition, sources and processes during wintertime in Beijing, China. Atmos. Chem. Phys. 13, 4577–4592.

Sun, Y.L., Zhuang, G.S., Tang, A.H., Wang, Y., An, Z.S., 2006. Chemical characteristics of PM2:5 and PM10 in haze-fog episodes in Beijing. Environ. Sci. Technol. 40 (10), 3148–3155.

Tan, Z.F., Fuchs, H., Lu, K.D., Hofzumahaus, A., Bohn, B., Broch, S., Dong, H.B., Gomm, S., Häseler, R., He, L.Y., Holland, F., Li, X., Liu, Y., Lu, S.H., Rohrer, F., Shao, M., Wang, B.L., Wang, M., Wu, Y.S., Zeng, L.M., Zhang, Y.S., Wahner, A., Zhang, Y.H., 2017. Radical chemistry at a rural site (Wangdu) in the North China Plain: observation and model calculations of OH, HO2 and RO2 radicals. Atmos. Chem. Phys. 17 (1), 1–48.

Tang, G.Q., Zhang, J.Q., Zhu, X.W., Song, T., Münkel, C., Hu, B., Schaefer, K., Liu, Z.R., Zhang, J.K., Wang, L.L., Suppan, P., Wang, Y.S., 2016. Mixing layer height and its implications for air pollution in Beijing, China. Atmos. Chem. Phys. 16 (4), 2459–2475.

Tuccella, P., Curci, G., Visconti, G., Bessagnet, B., Menut, L., Park, R.J., 2012. Modeling of gas and aerosol with WRF/Chem over Europe: evaluation and sensitivity study. J. Geophys. Res. Atmos. 117 (D3).

Vasilakos, P., Russell, A., Weber, R., Nenes, A., 2018. Understanding nitrate formation in a world with less sulfate. Atmos. Chem. Phys. 18 (17), 12765–12775.

Wang, G.H., Zhang, F., Peng, J.F., Duan, L., Ji, Y.M., Marrero-Ortiz, W., Wang, J.Y., Li, J.J., Wu, C., Cao, C., Wang, Y., Zheng, J., Secrest, J., Li, Y.X., Wang, Y.Y., Li, H., Li, N., Zhang, R.Y., 2018. Particle acidity and sulfate production during severe haze events in China cannot be reliably inferred by assuming a mixture of inorganic salts. Atmos. Chem. Phys. 18, 10123–10132.

Wang, G.H., Zhang, R.Y., Gomez, M.E., Yang, L.X., Zamora, M.L., Hu, M., Lin, Y., Peng, J.F., Guo, S., Meng, J.J., Li, J.J., Cheng, C.L., Hu, T.F., Ren, Y.Q., Wang, X.S., Gao, J., An, Z.S., Zhou, W.J., Li, G.H., Wang, J.Y., Tian, Y.Q., Marrero-Ortiz, W., Secrest, J., Du, Z.F., Zheng, J., Dongjie, S., Zeng, L., Shao, M., Wang, W.G., Huang, Y., Wang, Y., Zhu, Y.J., Li, Y.X., Hu, J.X., Pan, B., Cai, L., Cheng, Y.T., Ji, Y.M., Zhang, F., Rosenfeld, D., Liss, P.S., Duce, R.A., Kolb, C.E., Molinax, M.J., 2016a. Persistent sulfate formation from London Fog to Chinese haze. Proc. Natl. Acad. Sci. U.S.A. 48 (113), 13630–13635.

Wang, J., Hoffmann, A.A., Park, R.J., Jacob, D.J., Martin, S.T., 2008a. Global distribution of solid and aqueous sulfate aerosols: effect of the hysteresis of particle phase transitions. J. Geophys. Res. Atmos. 113, D11206.

Wang, J., Jacob, D.J., Martin, S.T., 2008b. Sensitivity of sulfate direct climate forcing to the hysteresis of particle phase transitions. J. Geophys. Res. Atmos. 113, D11207.

Wang, J., Park, S., Zeng, J., Ge, C., Yang, K., Carn, S., Krotkov, N., Omar, A.H., 2013. Modeling of 2008 Kasatochi volcanic sulfate direct radiative forcing: assimilation of OMI SO2 plume height data and comparison with MODIS and CALIOP observations. Atmos. Chem. Phys. 13, 1895–1912.

Wang, K., Zhang, Y., Nenes, A., Fountoukis, C., 2012. Implementation of dust emission and chemistry into the Community Multiscale Air Quality modeling system and initial application to an Asian dust storm episode. Atmos. Chem. Phys. 12, 10209–10237.

Wang, M.T., Zhu, B., Wang, H.L., Xue, G.Q., He, J., Xu, H.H., Cao, J.F., 2015. Composition and regional characteristics of atmosphere aerosol and its water soluble ions over the Yangtze River Delta region in a winter haze period. Environ. Sci. (7), 2337–2345 (in Chinese).

Wang, Y., Wang, J., Xu, X.G., Henze, D.K., Wang, Qu, Z., 2016b. A new approach for monthly updates of anthropogenic sulfur dioxide emissions from space: application to China and implications for air quality forecasts. Geophys. Res. Lett. 43, 9931.

Weber, R.J., Guo, H.Y., Russell, A.G., Nenes, A., 2016. High aerosol acidity despite declining atmospheric sulfate concentrations over the past 15 years. Nat. Geosci. 9, 282–286.

Yang, Y., Wang, H.L., Smith, S.J., Easter, R., Ma, P.L., Qian, Y., Yu, H.B., Rasch, P.J., 2017. Global source attribution of sulfate concentration and direct and indirect radiative forcing. Atmos. Chem. Phys. 17 (14), 8903–8922.

Yang, Y.R., Liu, X.G., Qu, Y., Wang, J.L., An, J.L., Zhang, Y.H., Zhang, F., 2015. Formation mechanism of continuous extreme haze episodes in the megacity Beijing, China, in January 2013. Atmos. Res. 155, 192–203.

Zaveri, R.A., Peters, L.K., 1999. A new lumped structure photochemical mechanism for large-scale applications. J. Geophys. Res. Atmos. 104, 30387–30415.

Zaveri, R.A., Easter, R.C., Fast, J.D., Peters, L.K., 2008. Model for simulating aerosol interactions and chemistry (MOSAIC). J. Geophys. Res. Atmos. 113, D13204.

Zaveri, R.A., Easter, R.C., Peters, L.K., 2005b. A computationally efficient multicomponent equilibrium solver for aerosols (MESA). J. Geophys. Res. 110, D24203.

Zaveri, R.A., Easter, R.C., Wexler, A.S., 2005a. A new method for multicomponent activity coefficients of electrolytes in aqueous atmospheric aerosols. J. Geophys. Res. 110, D02201.

Zdanovskii, A.B., 1948. New methods of calculating solubilities of electrolytes in multicomponent systems. Zh. Fiz. Khim. 22, 1475–1485.

Zhai, Y.R., Wang, Q.G., Song, Y.Y., 2012. Air pollutant emissions from energy consumptions in the Yangtze River Delta region. 2012. China Environ. Sci. 32 (9), 1574–1582 (in Chinese).

Zhang, Y., Carmichael, G.R., 1999. The role of mineral aerosol in tropospheric chemistry in East Asia – a model study. J. Appl. Meteorol. 38, 353–366.

Zheng, B., Zhang, Q., Zhang, Y., He, K.B., Wang, K., Zheng, G.J., Duan, F.K., Ma, Y.L., Kimoto, T., 2015. Heterogeneous chemistry: a mechanism missing in current models to explain secondary inorganic aerosol formation during the January 2013 haze episode in North China, Atmos. Chem. Phys. 15, 2031–2049.

Zhu, X.W., Tang, G.Q., Hu, B., Wang, L.L., Xin, J.Y., Zhang, J.K., Liu, Z.R., Münkel, C., Wang, Y.S., 2016. Regional pollution and its formation mechanism over north China plain: a case study with ceilometer observations and model simulations. J. Geophys. Res. Atmos. 121 (24) 14, 574-14, 588.